

Adversarial point perturbations on 3D objects

Daniel Liu¹, Ronald Yu², and Hao Su²

¹Torrey Pines High School, San Diego, CA

²University of California San Diego, La Jolla, CA

Abstract

The importance of training robust neural network grows as 3D data is increasingly utilized in deep learning for vision tasks, like autonomous driving. We examine this problem from the perspective of the attacker, which is necessary in understanding how neural networks can be exploited, and thus defended. More specifically, we propose adversarial attacks based on solving different optimization problems, like minimizing the perceptibility of our generated adversarial examples, or maintaining a uniform density distribution of points across the adversarial object surfaces. Our four proposed algorithms for attacking 3D point cloud classification are all highly successful on existing neural networks, and we find that some of them are even effective against previously proposed point removal defenses.

1 Introduction

Improving the resilience of neural networks against adversarial attacks is an important step in building more robust and secure models. Currently, both new attacks and new defensive techniques are being developed. Attacks are important for finding out how we can exploit the neural networks, and that allows us to craft better defenses. It also allows us to study the behavior of neural networks against out-of-distribution adversarial examples. Though adversarial attacks and defenses are well-studied for 2D images, they are only beginning to be examined in 3D space and other domains by making use of domain-specific insights.

3D data is important because it is used as an input for controlling autonomous driving systems and robotics. However, one hindrance in studying deep learning on 3D data is due to the different representation of 3D data, like voxels, point clouds, and meshes. We specifically look into the task of 3D point cloud classification, which involves feeding order-invariant point sets into neural networks. 3D point cloud data

can be obtained in many ways. For example, point clouds are produced in LiDAR (Light Detection and Ranging) scans, RGB-D scans, and photogrammetry of 3D objects. Point clouds can also be obtained through conversions from other data types, like 3D meshes or voxels.

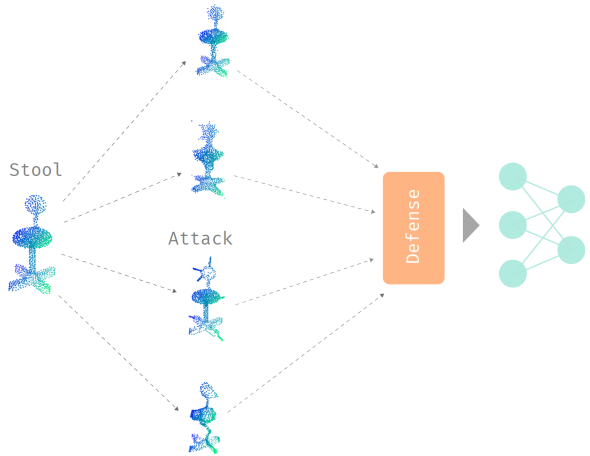


Figure 1: The adversarial attack and defense process with our four proposed attacks.

It is easy to create effective adversarial attacks. However, we are interested in crafting adversarial perturbations that satisfy certain criteria. For example, L_p norms are commonly used to bound the perceptibility, or the degree of change, in perturbations on 2D images. This allows the adversarial perturbations to be *human-imperceptible* if the change is small. In this paper, we want to exploit certain criteria that are only valid for 3D point clouds that describe the shape or surface of 3D objects in generating our adversarial examples. Therefore, we develop four new algorithms for attacking 3D deep learning:

- A distributional attack using projected gradient descent that attempts to maintain the shape of a 3D object that is represented as a point cloud.

- Two resampling-based attacks that attempt to modify the shape of a 3D object through vanilla gradient descent and resampling.
- A differentiable operation that changes the shape of a 3D point cloud by attracting points on the surface of the represented object, which can be directly optimized with efficient first order methods.

These algorithms are based on novel formulations of the optimization problems for generating adversarial examples, and we approximate solutions to them with different techniques. Naturally, our approaches differ from previous attacks created for 2D images because we take into consideration the intrinsic shape structure of the 3D points. A cartoon describing our algorithms is shown in Figure 2, and it provides a brief overview of the main steps in our algorithms.

We perform experiments on the PointNet [Qi et al., 2017b] and PointNet++ [Qi et al., 2017c] models with the ModelNet40 [Wu et al., 2015] dataset. We use point clouds that are sampled from the surface of the 3D objects with uniform density.¹

2 Related Work

2.1 Attacks

Szegedy et al. [2013] first examined how adversarial perturbations on 2D images could be generated on a neural network by searching for some perturbation that causes a neural network to make a wrong prediction. Goodfellow et al. [2014] later proposed a fast approximation for generating adversarial examples using one step gradient descent constrained by the L_∞ norm. This result was generalized by Madry et al. [2017] and Kurakin et al. [2016b,a] to obtain an attack that maximized the overall loss resulting from the perturbations, while bounding the magnitude of the perturbations by the L_p norm, for some p . This optimization problem is solved through multiple iterations of projected gradient descent, in what is sometimes known as the “iterative gradient attack”. There are many further improvements by Papernot et al. [2016a], Moosavi-Dezfooli et al. [2016], Dong et al. [2018], and Moosavi-Dezfooli et al. [2017] on perturbing 2D images. Carlini and Wagner [2017] proposed a different approach that minimizes both an objective function that represents the distance between the current prediction and the target class, and

¹The source code for this work is available at this [http url: <https://github.com/Daniel-Liu-c0deb0t/Adversarial-point-perturbations-on-3D-objects>](https://github.com/Daniel-Liu-c0deb0t/Adversarial-point-perturbations-on-3D-objects)

the perturbation’s L_p norm at the same time. Then, the neural network misclassifies into a specific target class.

In terms of understanding adversarial examples, Ilyas et al. [2019] discovered that adversarial examples are due to neural networks learning and relying on human-imperceptible features.

Only very recently has adversarial attacks been examined in 3D space. For 3D point clouds, Xiang et al. [2018], Yang et al. [2019], and Liu et al. [2019] all proposed point perturbations based on shifting points using ideas similar to attacks on 2D images. Xiang et al. [2018] also proposed an attack that generates clusters of points with different shapes. For this attack, they optimize an objective function that constrains the distance between the generated clusters and the main benign point cloud. Zheng et al. [2018] and Wicker and Kwiatkowska [2019] both proposed saliency-based techniques for removing points. An adversarial attack that perturbed the distribution of points on a 3D object’s surface was examined in Liu et al. [2019]. Adversarial attacks on LiDAR systems were proposed in Cao et al. [2019] by making the scanning operation that converts a triangular mesh into a point cloud differentiable.

2.2 Defenses

A popular defense for 2D image space is adversarial training, where a neural network is trained with adversarial examples [Goodfellow et al., 2014]. This is done by adding the loss incurred by adversarial examples to the objective function that is optimized throughout training. Another defensive technique is defensive distillation [Papernot et al., 2016b]. Later work has shown that a neural network can be trained to be provably robust [Wong and Kolter, 2017]. For neural networks that classify 3D point clouds, removing points was shown to be more effective than adversarial training. In particular, Liu et al. [2019] and Zhou et al. [2018] both examined removing outlier points, and Liu et al. [2019] also examined removing salient points. Liu et al. [2019] argued that these defenses were effective due to the special global max pooling operation in the PointNet [Qi et al., 2017b] and PointNet++ [Qi et al., 2017c] architectures that were evaluated, which provides some sort of gradient masking to hide some points against gradient-based perturbations.

2.3 3D Deep Learning

3D deep learning has recently experienced exponential growth. Many network architectures were proposed

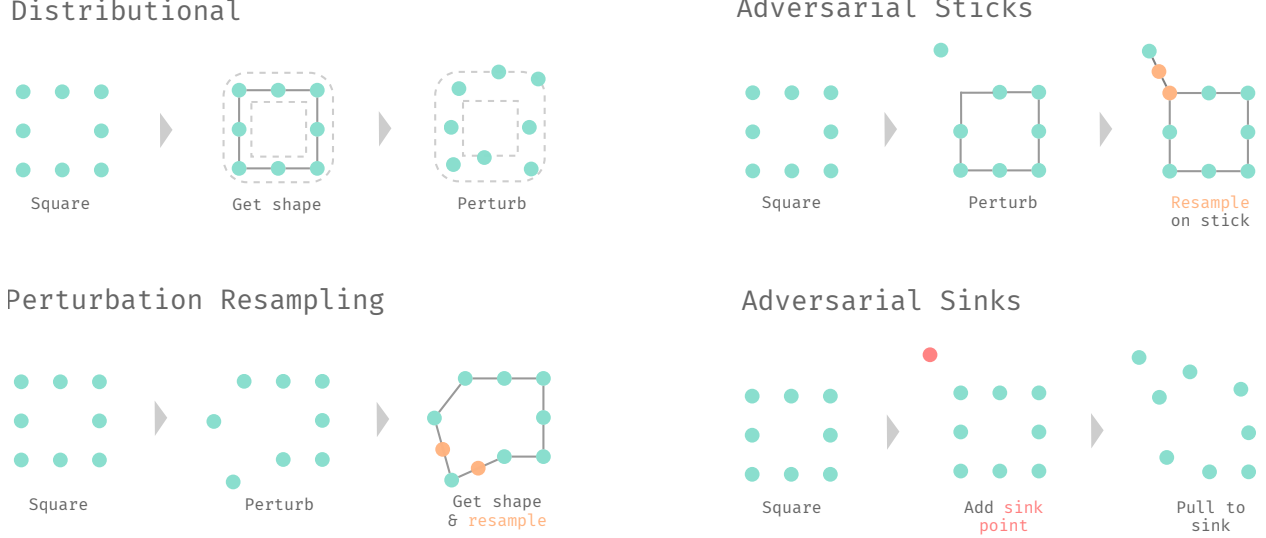


Figure 2: 2D cartoon describing the general idea for our four adversarial attacks. Note that in 3D, we estimate shapes through flat 3D triangles instead of line segments.

for different tasks in 3D deep learning.

We specifically examine the case of 3D point cloud classification. PointNet [Qi et al., 2017b] and PointNet++ [Qi et al., 2017c] are two architectures built specifically for learning from point sets. Other work on this task include Qi et al. [2017a] and Deng et al. [2018].

There is also work on handling voxel (quantized point cloud) data [Wang et al., 2017, Wu et al., 2015].

3 Setting

We have a neural network model $f_\theta : \mathbb{R}^{N \times 3} \mapsto \mathbb{R}^M$, which solves the 3D point cloud classification task by predicting probability vectors for each output class. It takes in x , a set of N 3D points, and outputs a vector $f_\theta(x)$ of length M that contains the probability of the input x being each output possible class. The model f_θ is trained by adjusting its parameters θ to minimize the cross entropy loss, which is denoted by $J(f_\theta(x), y)$, for each sample x and its corresponding one-hot label y that are drawn from the distribution D :

$$\underset{\theta}{\text{minimize}} \quad \mathbb{E}_{(x,y) \sim D} J(f_\theta(x), y) \quad (1)$$

In terms of notation, we will use vector and set operations on a point cloud interchangeably (for example, norm and set union operations), since a point cloud is a set of unique points, but we can also assign an arbitrary order to the points so it behaves like a vector. For a point set x , we can access its i -th element (point) through $x[i]$.

In terms of the threat model, we assume that the attacker has full access to the architecture and parameters θ of a neural network f_θ (white-box threat model). The attacker also has access to the unstructured 3D point clouds, which they can change before feeding them to the neural network. Therefore, we wish to construct attacks that are purely based on unstructured 3D point sets, without any extra shape or normal information on the structure of the point set. We will focus on generating *untargeted* attacks, where the attacker is attempting to force a neural network into misclassifying an object of a certain class into a different class.

In our experiments, we also evaluate defensive techniques. After we generate adversarial attacks on a clean/benign point cloud x by perturbing it with $\delta \in \mathbb{R}^{N \times 3}$ to obtain $x^* = x + \delta$, we feed x^* to a defense before it is classified by a neural network. The full attack and defense pipeline is shown in Figure 1.

We now discuss the outlier removal and salient point removal defenses from Liu et al. [2019] in more detail because they are used in our experiments. The outlier removal defense involves first calculating statistical outliers through

$$o[i] = \frac{1}{K} \sum_{j=1}^K \text{NN}(x^*[i], j), \quad \forall i \in \{1 \dots N\} \quad (2)$$

with $\text{NN}(\rho, j)$ returning the j -th nearest neighboring point of the point ρ . Then, we remove points greater than ϵ standard deviations away from the average $o[i]$

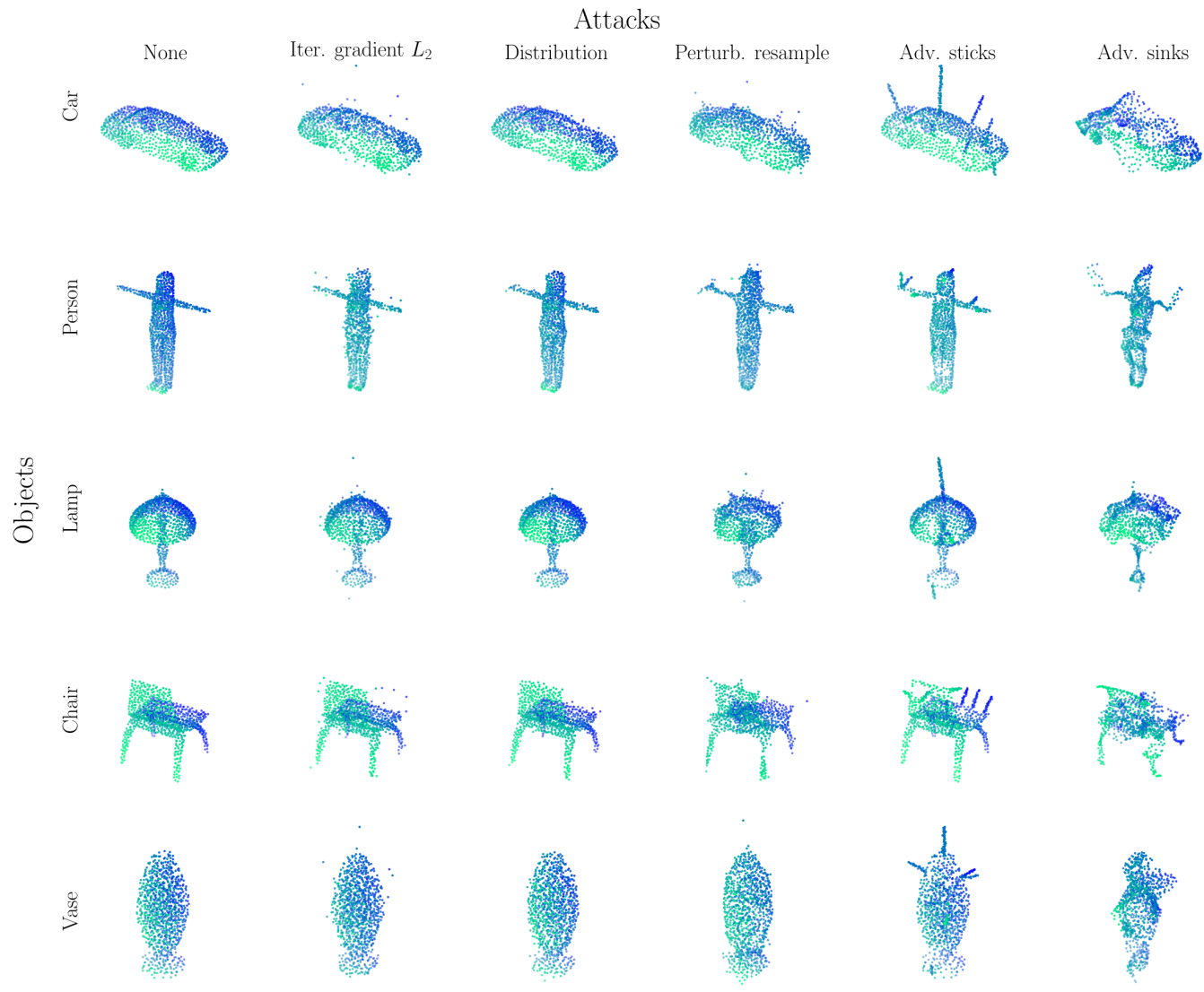


Figure 3: Visualizations of adversarial examples that are generated on the PointNet architecture, for five different ModelNet40 classes.

across all i :

$$x^{**} = x^* \setminus \left\{ x^*[i] : o[i] > \frac{1}{N} \sum_{j=1}^N o[j] + \epsilon \text{STDEV}(o) \wedge i \in \{1 \dots N\} \right\} \quad (3)$$

In the salient point removal defense, salient points are identified and removed by first calculating the saliency

$$s[i] = \max_{j \in \{1 \dots M\}} \left\| (\nabla_{x^*} f_\theta(x^*))[j] \right\|_2, \quad \forall i \in \{1 \dots N\} \quad (4)$$

and a subset of the points in x^* with the highest saliencies are removed.

4 Attack Types

In this paper, we examine two classes of attacks. The first type of attacks is constructed to perturb the distribution of points on or very near a 3D object. This allows the shape of an object to remain mostly unchanged, so the perturbations remain unnoticeable to humans. The second type of attacks we examine is focused on changing the shape of an object given only its point cloud, and we do not force the perceptibility of this attack to be extremely low.

These shape attacks have two main benefits. First, it is easier to construct an adversarial example with the shape attacks in real-life, because it is difficult to change the distribution of points obtained through a scanner, while changing the shape is considerably easier. Also, changing the shape is more realistic than creating outlier points that float far away from a 3D object in point-based attacks [Xiang et al., 2018, Liu et al., 2019]. Second, it is robust against point cloud restoration defenses that attempt to recover information about the shape of an adversarial point cloud based on the density of points. This is because the shape attacks are built to maintain uniform densities of points in the adversarial examples, so that they behave as if points were directly sampled from of a perturbed 3D object. Thus, any density information is essentially destroyed, so it is difficult to apply a defensive method that utilizes this special 3D property. Also, defending against attacks by removing points will not work, since removing a few points will not change the overall shape of a perturbed 3D object.

5 Distributional Attack

To craft a distributional attack, we need to first quantify the perceptibility of the adversarial perturba-

tions. Although the perceptibility of different adversarial perturbations is quite subjective to humans, we choose to quantify perceptibility by comparing a perturbed, adversarial point cloud to the true shape of the clean/benign surface point cloud, which is represented by a set of infinite points S . By comparing the adversarial point cloud to the true shape of the object, we can measure how far the perturbations cause the adversarial point cloud to deviate from the true shape it should be describing. This also allows us to ignore small changes to the density of points on the surface of the object, which do not disturb the overall shape of the object, and are thus deemed imperceptible.

More specifically, we use the Hausdorff distance between two sets A and B to quantify perceptibility:

$$\mathcal{H}(A, B) = \max_{a \in A} \min_{b \in B} \|b - a\|_2 \quad (5)$$

In other words, we want to find the maximum of the distances between each point in A and its closest point in B , where the Euclidean distance metric is used.

Note that the true surface S is usually approximated through a triangular mesh $t \in \mathbb{R}^{T \times 3 \times 3}$, with T triangles total. However, throughout this paper, we will often express ideas using the set S instead of its triangular mesh approximation, since a set is easier to manipulate. In practice, since triangular meshes are used instead of S , we define a distance metric \mathcal{D} that describes the distance between a set of points x , and a set of triangles t :

$$\mathcal{D}(x, t) = \max_{i \in \{1 \dots N\}} \min_{j \in \{1 \dots T\}} d(x[i], t[j]) \quad (6)$$

The distance $d(a, b)$ between a single point a and a single triangle b is defined as the distance between the point a and the closest point to a on the triangle b .

Our approach differs from that of Xiang et al. [2018], because we measure the amount of perturbation by comparing the perturbed point cloud x^* to S (or its approximation t), rather than the benign point cloud x . The benefit of our approach is that it is less sensitive to the density of points in x . Our method also differs from using an L_p norm to measure perceptibility, as L_p norms do not take the shape of a 3D object into account.

If we structure our optimization problem for constructing adversarial point clouds to minimize \mathcal{H} , then we can craft adversarial perturbations that are imperceptible. A naive formulation of the problem yields

$$\begin{aligned} & \underset{\delta}{\text{minimize}} \quad \mathcal{H}(x + \delta, S) \\ & \text{subject to} \quad \arg \max f_\theta(x + \delta) \neq \arg \max y \end{aligned} \quad (7)$$

However, this formulation is very hard to solve with gradient-based methods since the objective function

Algorithm 1 The distributional attack algorithm.

Input: x : input benign point cloud with N points, n : number of iterations, τ : maximum distance from S , and ϵ : amount of perturbation.

Output: x^* : adversarial point cloud.

```

 $tri \leftarrow$  Boundary triangles of the alpha shape of  $x$ 
 $tree \leftarrow$  Build a VP-tree on the triangles in  $tri$ 
 $x^* \leftarrow x$ 
for  $i \in \{1 \dots n\}$  do
     $\delta \leftarrow \frac{\epsilon}{n} \left( \frac{\nabla_{x^*} J(f_\theta(x^*), y)}{\|\nabla_{x^*} J(f_\theta(x^*), y)\|_2} \right)$ 
     $x^* \leftarrow x^* + \delta$ 
     $x^* \leftarrow$  Project each point in  $x^*$  to be within  $\tau$  distance away from the triangles in  $tri$ , using the VP-tree  $tree$ 
end for

```

and the constraint are not differentiable. Therefore, we reformulate this problem to maximize a smooth (differentiable) loss function:

$$\begin{aligned} & \underset{\delta}{\text{maximize}} \quad J(f_\theta(x + \delta), y) \\ & \text{subject to} \quad \mathcal{H}(x + \delta, S) \leq \tau \end{aligned} \quad (8)$$

This formulation is similar to the optimization problem solved through Madry et al. [2017]’s projected gradient descent, but with a different method for measuring perceptibility.

Now, we consider the special case where $\tau = 0$, and show that this leads to the previously proposed “gradient projection” attack. The effect of setting $\tau = 0$ is that the perturbations must not cause any points to move off the shape of the point cloud. If we attempt to simplify this further and constrain each point in x to be within the triangle in t that contains that point after perturbing x , then we obtain the previous gradient projection technique [Liu et al., 2019]. However, our goal is to solve this problem without simplifications, and without relying on the surface triangles that is assumed to be given in the input. Note that the constraint is still not differentiable, so we cannot directly apply gradient descent.

To solve this problem, we take inspiration from projected gradient descent [Madry et al., 2017], which is used in attacks on 2D images (*e.g.*, using $\max\{\min\{x + \delta, 1\}, 0\}$ to clip the perturbed pixels onto the proper range for each color channel), and attempt to project $x + \delta$ onto the set S at each step in the attack. Before projecting the perturbed points, we still need to calculate δ to perturb the points in arbitrary directions. Therefore, we can constrain the L_p norm (we use the L_2 norm) of the perturbations before projecting the perturbed points, in order to control the scale the perturbations through the hyperparameter ϵ . Thus,

the optimization problem can be solved by iterating

$$\begin{aligned} x_1^* &= x, \\ x_{i+1}^* &= \bigcup_{j=1}^N \left\{ \mathcal{P} \left(x_i^*[j] + \frac{\epsilon}{n} \left(\frac{(\nabla_{x_i^*} J(f_\theta(x_i^*), y))[j]}{\|\nabla_{x_i^*} J(f_\theta(x_i^*), y)\|_2} \right), S \right) \right\}, \\ & \quad \forall i \in \{1 \dots n-1\} \end{aligned} \quad (9)$$

for a projection function \mathcal{P} , which projects a perturbed point into the region around S . We can express this projection function as

$$\mathcal{P}(\rho, S) = \arg \min_{s \in \{a: \mathcal{H}(\{a\}, S) \leq \tau \wedge a \in \mathbb{R}^3\}} \|\rho - s\|_2 \quad (10)$$

Conceptually, we are convolving a sphere of radius τ with the surface S to obtain the set of all points within τ distance of S , through what is known as Minkowski addition.

There are a few problems with directly applying the aforementioned attack in practice:

1. We lack the true bounding shape of each input object, which is represented as t . We need some method to infer the triangles on the surface of a point cloud x . This inferred shape does not need to be extremely accurate—an approximation will suffice as long as the projected perturbations are not noticeable.
2. There is significant overhead from naively examining each triangle in t to find the nearest possible projection point. The entire operation has a time complexity of $O(NT)$ with respect to each constant-time projection operation, which hinders the scalability of the attack as the number of point clouds and the number of points increases.

The first problem can be solved by constructing a triangulation of the surface of an input object through its 3D point cloud. We choose to construct the alpha

shape [Edelsbrunner et al., 1983] of the point cloud and obtain the boundary triangles, though there are other triangulation methods like the ball-pivoting algorithm [Bernardini et al., 1999]. The alpha shape algorithm involves first computing a 3D Delaunay triangulation [Lee and Schachter, 1980] of the point cloud to obtain a set of tetrahedrons, and then removing tetrahedrons with circumscribing spheres of radius greater than the constant parameter α . In our experiments, we use the average distance between each point and its adjacent points in the Delaunay triangulation as the α value.

To speed up projection queries, we can build some sort of data structure to store the triangles that we are projecting onto. Let us bound the triangle $t[i]$ with a circle of radius $r[i]$ and center $c[i]$, $\forall i \in \{1 \dots T\}$. Then, we can represent each triangle with its corresponding center point $c[i]$, for some i . We build a VP-tree [Yianilos, 1993], which recursively partitions a metric space with circles, on the points c . When we project a point ρ that is perturbed by a vector δ , we only project $\rho + \delta$ onto triangles whose centers lie in a sphere centered at ρ with radius $R = \|\delta\|_2 + \tau + \max_{i \in \{1 \dots T\}} r[i]$. This is because we assume that the point ρ lies within a triangle before it is perturbed, and so that triangle must lie in the sphere with radius R and centered at $\rho + \delta$. We do not need to examine any triangles farther away if we are guaranteed to encounter at least one triangle within the radius R .

The full algorithm for the distributional attack is summarized in Algorithm 1. Note that the triangulation and VP-tree algorithms will be used later for other attacks.

6 Shape Attacks

We want to perturb the shape of an object to generate effective attacks, which is the opposite of the distributional attack. These shape attacks have the benefit of being more realistic and also more robust against 3D point cloud specific defenses, instead of being imperceptible. However, constructing these attacks is nontrivial because we only have access to a set of points x that is sampled from the true shape of the object. The general idea behind each of our proposed shape attacks is that we ensure that points are evenly sampled on the resulting shape implicitly represented by the point cloud x . We define an even sampling that results in the points $x \subset S$ on a surface represented by S as ensuring that the distances between each point and its nearest neighboring point in x is the maximum possible so clusters of points do

not form. In other words, we want the *density* of the sampled points to be as uniform as possible on S .

We present three attacks that form three different perspectives on how we can maintain the uniform density of points. The first algorithm, perturbation resampling, is a straightforward realization of the idea of enforcing an even sampling after perturbing the shape of a point cloud. Then, we propose a method to add additional adversarial structures (sticks) to a 3D object. These two methods rely on inferring the overall shape of a point cloud and resampling, which are both nondifferentiable. Finally, we propose a fully differentiable attack for perturbing the shape represented by a point cloud without first attempting to estimate the overall shape of the point cloud.

6.1 Perturbation Resampling

Consider an adversarial object’s surface that is represented by the set S^* , and its benign surface which is represented S . We want to ensure that the point distribution of a point cloud $x^* \subset S^*$ is even on this surface. This idea can be expressed through the following optimization problem:

$$\begin{aligned} \underset{x^*, S^*}{\text{maximize}} \quad & J(f_\theta(x^*), y) \\ & + \lambda \min_{i \in \{1 \dots N\}} \min_{j \in \{1 \dots N\} \setminus \{i\}} \|x^*[j] - x^*[i]\|_2 \\ \text{subject to} \quad & \mathcal{H}(S^*, S) \leq \epsilon, \\ & x^*[k] \in S^*, \quad \forall k \in \{1 \dots N\} \end{aligned} \tag{11}$$

In other words, we want to change the shape S^* to maximize the loss $J(f_\theta(x^*), y)$, but we also want to maximize the distance between each point in x^* and its nearest point as much as possible. However, it is hard to directly optimize using gradient-based methods to solve this problem due to the highly nonlinear objective function. Therefore, we seek to construct an acceptable approximation of the solution x^* through farthest point sampling.

We use farthest point sampling on a large subset of randomly sampled points from S^* to obtain a set of points with approximately uniform density on S^* . Farthest point sampling allows us to pick a new point that is the farthest away from previously picked points in each iteration of the algorithm, which leads to a greedy approximation to maximizing the minimum distances between each point and its nearest neighboring point. In practice, the points are sampled from an approximation of S^* that is obtained through the alpha shape algorithm.

During each iteration of the perturbation resampling attack, we first execute one step of gradient descent constrained by the L_2 norm and perturb the point

Algorithm 2 The perturbation resampling algorithm.

Input: x : input benign point cloud with N points, n : number of iterations, ϵ : amount of perturbation, and κ : number of points to resample.

Output: x^* : adversarial point cloud.

```

 $x^* \leftarrow x$ 
for  $i \in \{1 \dots n\}$  do
   $\delta \leftarrow \frac{\epsilon}{n} \left( \frac{\nabla_{x^*} J(f_\theta(x^*), y)}{\|\nabla_{x^*} J(f_\theta(x^*), y)\|_2} \right)$ 
   $x^* \leftarrow x^* + \delta$ 
   $tri \leftarrow$  Boundary triangles of the alpha shape of  $x^*$ 
   $\mathcal{R}(v) = \left| \{j : \|\delta[j]\|_2 \leq v \wedge j \in \{1 \dots N\}\} \right|$  ▷ Statistical rank of  $v$ .
   $sampled \leftarrow$  Farthest point sampling on  $tri$  for  $\kappa$  points, starting with the points in
   $\{x^*[j] : \kappa + 1 \leq \mathcal{R}(\|\delta[j]\|_2) \leq N \wedge j \in \{1 \dots N\}\}$ 
   $x^* \leftarrow \{x^*[j] : \kappa + 1 \leq \mathcal{R}(\|\delta[j]\|_2) \leq N \wedge j \in \{1 \dots N\}\} \cup sampled$ 
end for

```

cloud. Then, we approximate the shape of this perturbed point cloud by computing the alpha shape. Finally, we use farthest point sampling to resample the κ points with the lowest saliences, which is defined as the L_2 norm of the gradient of the loss function wrt each point. The $N - \kappa$ points with higher saliences are automatically considered “picked” from sampling. The full algorithm is sketched in Algorithm 2. We are essentially perturbing the underlying shape of the 3D point cloud, while ensuring that points are evenly sampled on the surface of that shape when the surface is stretched due to the perturbations.

One drawback of this attack is that the total perturbation $x^* - x$ is not directly bounded by ϵ under the original L_2 norm used in gradient descent. This is due to the resampling operation that may arbitrarily shift each of the κ points. In practice, this attack does not generate large, perceptible changes since the resampling operation only shifts points on the surface of the perturbed object. Another drawback is that intuitively, optimizing using gradient descent to increase $J(f_\theta(x^*), y)$ is hard, since resampling points arbitrarily shifts the position of the point cloud on the loss wrt input surface in each iteration. Furthermore, momentum and acceleration cannot be used in gradient descent due to the arbitrary jumps in our position while optimizing. However, in practice, we find that the success rate of this attack is high with just a few iterations of basic gradient descent.

6.2 Adversarial Sticks

We can attempt to create new features on the mesh instead of making small, incremental deformities through the perturbation resampling attack. Xiang et al. [2018] explores this idea by adding clusters of points and even 3D objects from other classes to at-

tack a benign 3D object. However, their attack does not enforce any connection between the benign object and the added clusters of points. In other words, the crafted adversarial example can contain many disjoint point clouds. We think that this is unrealistic for a classification task on a single point cloud object, so we attempt to add a new feature (sticks, or line segments) onto a point cloud, where the sticks must originate from the surface of the benign 3D object.

A straightforward formulation of the problem results in optimizing the position vector $\alpha \in \mathbb{R}^{\sigma \times 3}$, orientation and length vector $\beta \in \mathbb{R}^{\sigma \times 3}$, for generating σ sticks:

$$\begin{aligned}
 & \underset{\alpha, \beta}{\text{maximize}} \quad J(f_\theta(x \cup \mathcal{S}_\kappa(\alpha, \alpha + \beta)), y) \\
 & \text{subject to} \quad \|\beta\|_2 \leq \epsilon, \\
 & \quad \alpha[k] \in S, \quad \forall k \in \{1 \dots \sigma\}
 \end{aligned} \tag{12}$$

Note that $\mathcal{S}_\kappa(\alpha, \alpha + \beta)$ samples κ points across the line segments defined by the points $\alpha[i]$ and $\alpha[i] + \beta[i]$, $\forall i \in \{1 \dots \sigma\}$. The sampling procedure involves assigning points to each stick with probability proportional to its length, and then all points assigned to a stick are evenly spread out along the stick. These sampled points are added to the point cloud x , and they represent sticks that are connected to the point cloud. However, solving this is difficult due to a number of factors. First, the sampling function \mathcal{S} is not differentiable, which means that the objective function cannot be directly maximized. Second, we need to somehow constrain the position of each stick onto the surface of the benign point cloud x in each step of the attack.

We want to eliminate these two problems. The first problem can be solved by approximating the solution to the optimization problem by perturbing points based on saliency (L_2 norm of gradients) instead of

Algorithm 3 The adversarial sticks algorithm.

Input: x : input benign point cloud with N points, n : number of iterations, σ : number of sticks, ϵ : amount of perturbation, and κ : number of points to resample onto the sticks.

Output: x^* : adversarial point cloud.

```

 $x^* \leftarrow x$ 
for  $i \in \{1 \dots n\}$  do
   $\delta \leftarrow \frac{\epsilon}{n} \left( \frac{\nabla_{x^*} J(f_\theta(x^*), y)}{\|\nabla_{x^*} J(f_\theta(x^*), y)\|_2} \right)$ 
   $x^* \leftarrow x^* + \delta$ 
   $\mathcal{R}(v) = \left| \{j : \|\delta[j]\|_2 \leq v \wedge j \in \{1 \dots N\}\} \right|$  ▷ Statistical rank of  $v$ .
   $\Delta \leftarrow \{x^*[j] : N - \sigma + 1 \leq \mathcal{R}(\|\delta[j]\|_2) \leq N \wedge j \in \{1 \dots N\}\}$ 
   $x^* \leftarrow \{x[j] : \kappa + 1 \leq \mathcal{R}(\|\delta[j]\|_2) \leq N \wedge j \in \{1 \dots N\}\} \cup \mathcal{S}_\kappa \left( \bigcup_{k=1}^{\sigma} \{\mathcal{P}(\Delta[k])\}, \Delta \right)$ 
end for

```

orienting sticks. The assumption here is that perturbing a few points and then connecting those points to their closest points on the surface of the benign point cloud is an effective alternative to controlling the direction of sticks on the surface of the point cloud. To solve the second problem, we sample points on the generated sticks at the end, after directly perturbing points based on the gradient of f_θ . Also, instead of adding new points to the point cloud, we directly resample points with low saliences to the sticks. In summary, we use gradient descent constrained with the L_2 norm to attack the point cloud x , pick the σ points with the largest perturbations (saliencies), and sample points on the line segments defined by each perturbed point and its closest point (projection) on the surface of the benign point cloud. The full algorithm is given in Algorithm 3.

There are two main problems with this attack, similar to the perturbation resampling attack. First, the perturbations are no longer constrained by some ϵ under the L_2 norm after resampling some points, though we can still control the magnitude of the perturbation by tweaking the ϵ value for the gradient descent attack before sampling. Second, the sampling operation causes our location on the loss wrt input surface to jump arbitrarily during optimization, like the perturbation resampling attack. It is possible for the loss $J(f_\theta(x^*), y)$ to decrease after sampling points on the adversarial sticks, while we want the loss to stay the same or increase. This loss decrease is rare or insignificant in practice, since we find that the success rate of this attack is high in our experiments.

6.3 Resampling During Gradient Descent

The effectiveness of the perturbation resampling and adversarial sticks attack is still unexplained because of

the sampling operations that are interleaved with basic gradient descent steps. Therefore, we wish to build some intuition on why resampling points as described in the two previous attacks should not significantly decrease the higher loss attained through the basic gradient descent attack, if we assume that the neural networks are highly linear.

Consider the general architecture of the PointNet [Qi et al., 2017b] and PointNet++ [Qi et al., 2017c] networks, which is expressed as

$$f_\theta(x) = h_{\theta_2} \left(\text{MAX}_{i \in \{1 \dots N\}} g_{\theta_1}(x[i]) \right) \quad (13)$$

with g_{θ_1} representing a learnable nonlinear transformation on each point in x , and h_{θ_2} outputting a probability vector for each output class. In this case global MAX operation is performed element-wise (*i.e.*, maximum along each dimension) and produces a feature vector. Our analysis will focus on the global max pooling operation. We define a point $x[i]$ as being selected by the max pooling operation iff $\exists j : g_{\theta_1}(x[i])[j] = \text{MAX}_{k \in \{1 \dots N\}} g_{\theta_1}(x[k])[j]$.

For example, consider the simplified case where only one point is perturbed away from the initial benign point cloud, and that leads to an adversarial example which causes a neural network to mispredict. The perturbed point must be selected by the max pooling operation, since otherwise it cannot increase the loss, which is necessary in misprediction. In order for this perturbation to be effective, the neural network must also ignore (not select with the max pooling operation) existing, unperturbed points near the perturbed point, and the network is forced to pay attention to the perturbed point instead of other points in its local spatial region. This observation hints that the resampling operations in perturbation resampling and adversarial sticks mostly results in redundant points that are purely for visual purposes (*e.g.*, points are

evenly distributed on the surface of the point cloud). This is important because it shows that we are not jumping around by arbitrary amounts on the loss wrt input surface due to resampling while using gradient descent to craft the attacks.

Let us examine a simple case where the function g_{θ_1} is defined as

$$g_{\theta_1}(x[i]) = \psi(Wx[i] + B), \quad \forall i \in \{1 \dots N\} \quad (14)$$

In other words, we apply a nonlinearity (ReLU, or $\psi(z) = \max(0, z)$) to each point $x[i]$ after it undergoes an affine transformation. Note that in practice, there will be multiple layers of transformations. Now, if we assume that $Wx[i] + B > 0, \forall i \in \{1 \dots N\}$, then we just have the affine transformation. Goodfellow et al. [2014] argued that neural networks avoid the nonsaturating (flat) part of the ReLU function throughout training, which causes neural networks to behave linearly, so this is a reasonable assumption. The important property of affine transformations that we need is that it preserve lines and planes, and the ratio of distances between points before and after an affine transformation.

Consider a line segment made up of a set of colinear points x , which starts at point u and ends at point v . Note that if we compute $\text{MAX}_{k \in \{1 \dots N\}} x[k]$, the only points selected by the elementwise max operation will be the endpoints u or v , if we will ignore the rare cases where the line segment is exactly parallel to an axis. In this case, we define a point $x[i]$ as being selected iff $\exists j : x[i][j] = \text{MAX}_{k \in \{1 \dots N\}} x[k][j]$. After an affine transformation, the points are still colinear, and the points u and v are maintained as endpoints with all other points in between u and v on the line segment due to the ratio of distances between points being preserved. The points u and v are still the only points that can be selected by the max operation because they are the endpoints. We can directly extend this idea to the general case with multiple line segments in the adversarial sticks attack. If the PointNet and PointNet++ networks are mostly kept in the nonsaturating part of the ReLU function, then there is a high probability that sampling new points on the sticks (line segments) will not affect the points that are chosen by the max pooling operation, and thus they will not affect the network’s prediction.

For perturbation resampling, we sample points on triangles that have points perturbed through gradient descent as vertices. If we have a set of points x that represents the vertices (a , b , and c) of the triangle and a few other points sampled within the triangle, then $\text{MAX}_{k \in \{1 \dots N\}} x[k]$ will only select the vertices a , b , or c of the triangle, except for a few rare cases where the edges are parallel to an axis, similar to

the line segments. After an affine transformation on x , the result will still represent a triangle with the vertices a , b , and c at different locations, and all other sampled points within that triangle, similar to the line segments case. This is also due to the ratio of the distances between points being preserved in an affine transformation. Therefore, those vertex points will still be the only points selected by the elementwise max pooling operation after an affine transformation (and ReLU). In general, even with multiple triangles, points sampled within each triangle will very likely not affect the output of the neural network if it is highly linear.

The consequence of resampled points in a point cloud being ignored by the max pooling operation is that each resampling operation will move the location of the point cloud on the loss wrt input surface, but it will not change the loss. More specifically, consider the level set $\{x^* : J(f_\theta(x^*), y) = \ell \wedge x^* \in \mathbb{R}^{N \times 3}\}$, where we have attained a loss of ℓ so far due to gradient descent. Resampling points in x^* is essentially moves x^* to another point in the level set, as the loss stays the same because the resampled points do not affect the output of the neural network.

We show an example of the adversarial sticks attack in Figure 4. The sticks do have many points with zero gradients, but there are also points with nonzero gradients, which is due to PointNet’s nonlinearity. Later, we will show that even though some resampled points have nonzero gradients, resampling with gradient descent is able to generate effective adversarial attacks.

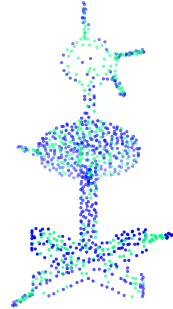


Figure 4: Example of the adversarial sticks attack on PointNet, with the stool object. Points with gradient equal to zero across all three dimensions are green. Notice that there are many points with zero gradients the adversarial sticks, but there are also a few points with nonzero gradients.

Interestingly, we show that attacks are also able to exploit the max pooling operation, as previously,

the global max pooling operation was shown to be helpful when removing points for defending against adversarial attacks [Liu et al., 2019]. We note that our assumptions about the high degree of linearity of neural networks is not likely in practice, but it gives theoretically guarantees about our algorithm in a specific scenario that may extend to the general case of nonlinear transforms that is harder to analyze.

6.4 Adversarial Sinks

We can deform the shape of the benign point cloud to generate an adversarial example without inferring its surface. We guide this deformation through sink points, which pull points in the point cloud in a local spatial region towards them. The reason for guiding the deformation process with a few points is because we want local changes to the shape of the point cloud that moves points that are selected by the max pooling operation. In other words, we want to minimize global changes to points that are not selected by the max pooling operation, as the max pooling operation is able to ignore a significant subset of points [Qi et al., 2017b].

Given a set of σ sink points $s_f \in \mathbb{R}^{\sigma \times 3}$ that are initialized with $s_0 \in \mathbb{R}^{\sigma \times 3}$, we can deform the point cloud x to create x^* with

$$\begin{aligned} x^*[i] &= x[i] \\ &+ \tanh \left(\sum_{j=1}^{\sigma} (s_f[j] - x[i]) \phi_{\mu'}(\|s_0[j] - x[i]\|_2) \right), \\ \forall i &\in \{1 \dots N\} \end{aligned} \tag{15}$$

where $\phi_{\mu'}$ represents a radial basis function that decreases the influence of each sink point by distance. This means that points in the point cloud that are far away from a sink point's initial position will be influenced less by that sink point as it moves. We use the Gaussian radial basis function which is defined as

$$\phi_{\mu'}(r) = e^{-\left(\frac{r}{\mu'}\right)^2} \tag{16}$$

for

$$\mu' = \frac{\mu}{N} \sum_{i=1}^N \min_{j \in \{1 \dots N\} \setminus \{i\}} \|x[j] - x[i]\|_2 \tag{17}$$

The hyperparameter μ can be tuned to control how the influence of each sink point falls off as distance increases. The influence of each sink point is also scaled by the average distance between point in x and its nearest neighboring point, so it is invariant to the scale of the point cloud x . We choose the Gaussian

radial basis function because it is differentiable everywhere and it outputs a value between 0 and 1, which represents a percentage of the distance between each point cloud point and sink point. In essence, Equation 15 represents shifting each point in the point cloud by the weighted sum of the vectors from that point to each sink point.

We can move the positions of the sink points to increase the overall loss. Essentially, we want to solve the following optimization problem:

$$\underset{s_f}{\text{maximize}} \quad J(f_\theta(x^*), y) - \lambda \|x^* - x\|_2 \tag{18}$$

where x^* is constructed according to Equation 15. The idea is that we are trying to maximize the overall loss by shifting our sink points s_f , while minimizing the L_2 norm of the perturbation. The hyperparameter λ can be adjusted to balance the emphasis on maximizing the loss and minimizing the L_2 norm of the perturbation. Unlike previous attacks that involve resampling, the perturbation operation on x with the sinks points s_f is fully differentiable wrt s_f :

$$\begin{aligned} \frac{\partial J(f_\theta(x^*), y)}{\partial s_f} &= \bigcup_{i=1}^{\sigma} \left\{ \sum_{j=1}^N (\nabla_{x^*} J(f_\theta(x^*), y))[j] \right. \\ &\quad \odot \tanh' \left(\sum_{k=1}^{\sigma} (s_f[k] - x[j]) \phi_{\mu'}(\|s_0[k] - x[j]\|_2) \right) \\ &\quad \left. \cdot \phi_{\mu'}(\|s_0[i] - x[j]\|_2) \right\} \end{aligned} \tag{19}$$

Therefore, we can directly apply a gradient-based optimization algorithm like Adam [Kingma and Ba, 2014] to maximize our objective function. In Equation 19, we see that the gradient wrt a sink point is scaled using the function $\phi_{\mu'}$, so points farther away from that sink point contribute less to how that sink point is moved during optimization.

It is important to tune λ to ensure that the magnitude of the perturbation stays plausible. To this end, we also apply \tanh' element-wise to the perturbation vector of each point in order to bound the perturbation with the horizontal asymptotes of the \tanh function.

Now, the question of how we initialize s_f and s_0 remains. We can examine the saliency of each point in x , which is given by the L_2 norm of the gradient of the loss of a neural network with respect to that point. Then, we can choose σ points with the highest saliencies and use their locations as the initial values for s_f and s_0 .

The full algorithm is shown in Algorithm 4.

Algorithm 4 The adversarial sinks algorithm.

Input: x : input benign point cloud with N points, n : number of iterations, σ : number of sinks, η : learning rate, λ : coefficient of the perceptibility term, and μ : coefficient of the falloff of the influence of each sink point.

Output: x^* : adversarial point cloud.

$$\begin{aligned} \mu' &\leftarrow \frac{\mu}{N} \sum_{i=1}^N \min_{j \in \{1 \dots N\} \setminus \{i\}} \|x[j] - x[i]\|_2 \\ \delta &\leftarrow \nabla_x J(f_\theta(x), y) \\ \mathcal{R}(v) &= \left| \{i : \|\delta[i]\|_2 \leq v \wedge i \in \{1 \dots N\}\} \right| \quad \triangleright \text{Statistical rank of } v. \\ s_0 &\leftarrow \{x[i] : N - \sigma + 1 \leq \mathcal{R}(\|\delta[i]\|_2) \leq N \wedge i \in \{1 \dots N\}\} \\ s_f &\leftarrow s_0 \\ C_{s_0}(s_f) &= J\left(f_\theta\left(\bigcup_{i=1}^N \left\{x[i] + \tanh\left(\sum_{j=1}^\sigma (s_f[j] - x[i])\phi_{\mu'}(\|s_0[j] - x[i]\|_2)\right)\right\}\right), y\right) \\ P_{s_0}(s_f) &= \left\| \bigcup_{i=1}^N \left\{ \tanh\left(\sum_{j=1}^\sigma (s_f[j] - x[i])\phi_{\mu'}(\|s_0[j] - x[i]\|_2)\right) \right\} \right\|_2 \\ \text{Find } s_f \text{ that maximizes } C_{s_0}(s_f) - \lambda P_{s_0}(s_f), \text{ with } n \text{ iterations of Adam (learning rate } = \eta) \\ x^* &\leftarrow \bigcup_{i=1}^N \left\{x[i] + \tanh\left(\sum_{j=1}^\sigma (s_f[j] - x[i])\phi_{\mu'}(\|s_0[j] - x[i]\|_2)\right)\right\} \end{aligned}$$

		Attacks					
		None	Iter. gradient L_2	Distributional	Perturb. resample	Adv. sticks	Adv. sinks
Defenses							
None	None	0.0%	97.9%	83.7%	95.5%	87.6%	89.4%
	Remove outliers	5.1%	55.6%	43.7%	82.8%	87.8%	82.6%
	Remove salient	6.7%	55.1%	38.5%	84.9%	89.4%	88.0%
$\mathcal{H}(x^*, S)$		0	0.352	0.053	0.326	0.353	0.377
Gradient = 0		36.7%	44.4%	39.1%	39.1%	35.5%	43.1%
Resampled gradient = 0		-	-	-	32.4%	54.5%	-

Table 1: The success rates of untargeted adversarial attacks against different defenses on the PointNet architecture. The attack with the highest success rate against each defense is bolded. The average Hausdorff distance $\mathcal{H}(x^*, S)$ between adversarial examples generated through each attack and the true object shapes are shown in the third to last row. The average percentage of points that have gradients across all dimensions equal to zero for each attack are shown in the second to last row. The average percentage of resampled points that have gradients across all dimensions equal to zero are shown in the last row for the perturbation resampling and adversarial sticks attacks.

7 Results

7.1 Setup

Models. We train PointNet [Qi et al., 2017b] and PointNet++ [Qi et al., 2017c] with default hyperparameters, but we use a slightly lowered batch size for PointNet++.

Dataset. The neural networks are trained on the training split of the ModelNet40 dataset [Wu et al., 2015]. The test split of the dataset is used for evaluating our adversarial attacks. We use point clouds of size $N = 1,024$ sampled with uniform density from 3D triangular meshes in the ModelNet40 dataset, and assume that the 3D triangular meshes represent the true shapes (S).

Attacks. For the traditional iterative gradient L_2 attack, we use $\epsilon = 3$ and $n = 10$ iterations. For the distributional attack, we use $\epsilon = 1$, $\tau = 0.05$, and $n = 10$ iterations. For perturbation resampling, we use $\epsilon = 3$, we resample $\kappa = 500$ points, and we run the attack for $n = 10$ iterations. For adversarial sticks, we use $\epsilon = 3$, we add $\sigma = 10$ sticks, and we resample $\kappa = 200$ points. For adversarial sinks, we use a learning rate of $\eta = 0.1$ for the Adam optimizer ($\beta_1 = 0.9$ and $\beta_2 = 0.999$), we scale the strength of each sink point by $\mu = 5$, we balance the objectives using $\lambda = 30$, and we run the attack for $n = 100$ iterations with $\sigma = 100$ sink points. Unlike previous work [Carlini and Wagner, 2017], we do not perform binary search on λ for a fair comparison against the other attacks.

Defenses. For removing outliers, we calculate the average distance from each point to its 10 nearest neighbors, and remove points with an calculated average distance greater than one standard deviation from the average of the average distances across all points. For removing salient points, we remove the 200 points with the highest saliencies. We do not test adversarial training because it is not attack agnostic and it was found to perform worse than the point removal defenses [Liu et al., 2019].

7.2 Adversarial Attacks

In Table 1, we show the success rates of our attacks on the 2,193 correctly classified objects from the ModelNet40 dataset, against the PointNet architecture with different defenses. Adversarial examples are visualized in Figure 5 and Figure 3.

We also show the success rates of our attacks on 2,220 objects that are correctly classified by PointNet++, in Table 2.

We show the success rate of the adversarial attacks as we increase the the number of points that are removed in the outlier removal and salient point removal defenses in Figure 6.

Success rates. The adversarial attacks we evaluated on PointNet were all highly successful without any defenses. The iterative gradient L_2 attack attained the highest success rate of 97.9%, while the distributional attack resulted in the lowest success rate of 83.7%. This was expected, since the distributional attack significantly limits the perceptibility of the perturbation. On PointNet++, the adversarial sticks attack did not perform well as it only reached a success rate of 41.3%. This is probably due to PointNet++ ignoring the few, large adversarial sticks as it locally groups points. Other attacks, like adversarial sinks, perturbation resampling, and the distributional attack result in higher success rates on PointNet++ than PointNet. The success rate of the distributional attack is over 10% higher on PointNet++, which suggests that PointNet++ is weaker against local spatial attacks. On both PointNet and PointNet++, resampling attacks (perturbation resampling and adversarial sticks) obtained lower success rates than the iterative gradient L_2 attack that did not have resampling, which means that resampling a fraction of the points does inhibit gradient descent and decrease the overall loss that we want to maximize in attacks. However, they were still able to obtain relatively high success rates on PointNet with just 10 iterations of gradient descent. The difference in the success rates between adversarial sticks and perturbation resampling attacks on PointNet is due to only 10 sticks being generated, while 524 points are perturbed with gradient descent in perturbation resampling.

If we apply a defensive technique after each attack, then the success rates of the iterative gradient L_2 and the distributional attack are reduced by approximately two to three times on both networks. The three shape attacks are much more resilient against point removal defenses, and they maintain success rates of between 80% and 90% on PointNet. On PointNet++, perturbation resampling and adversarial sinks maintain success rates slightly higher against the defenses compared to the same attacks on PointNet. Adversarial sticks obtains the highest success rate across all of the attacks we test against a defended PointNet, while adversarial sinks performs the best against a defended PointNet++. Interestingly, after applying a defense to the adversarial sticks attack, the success rate of the

		Attacks					
		None	Iter. gradient L_2	Distributional	Perturb. resample	Adv. sticks	Adv. sinks
Defenses	None	0.0%	100.0%	95.9%	98.8%	41.3%	94.1%
	Remove outliers	11.4%	47.6%	30.1%	84.4%	48.2%	94.3%
	Remove salient	11.0%	61.9%	28.2%	85.4%	50.2%	93.8%
$\mathcal{H}(x^*, S)$		0	0.159	0.050	0.173	0.162	0.272

Table 2: The success rates of untargeted adversarial attacks against different defenses on the PointNet++ architecture. The average Hausdorff distance $\mathcal{H}(x^*, S)$ between adversarial examples generated through each attack and the true object shapes are shown in the last row. The attack with the highest success rate against each defense is bolded.

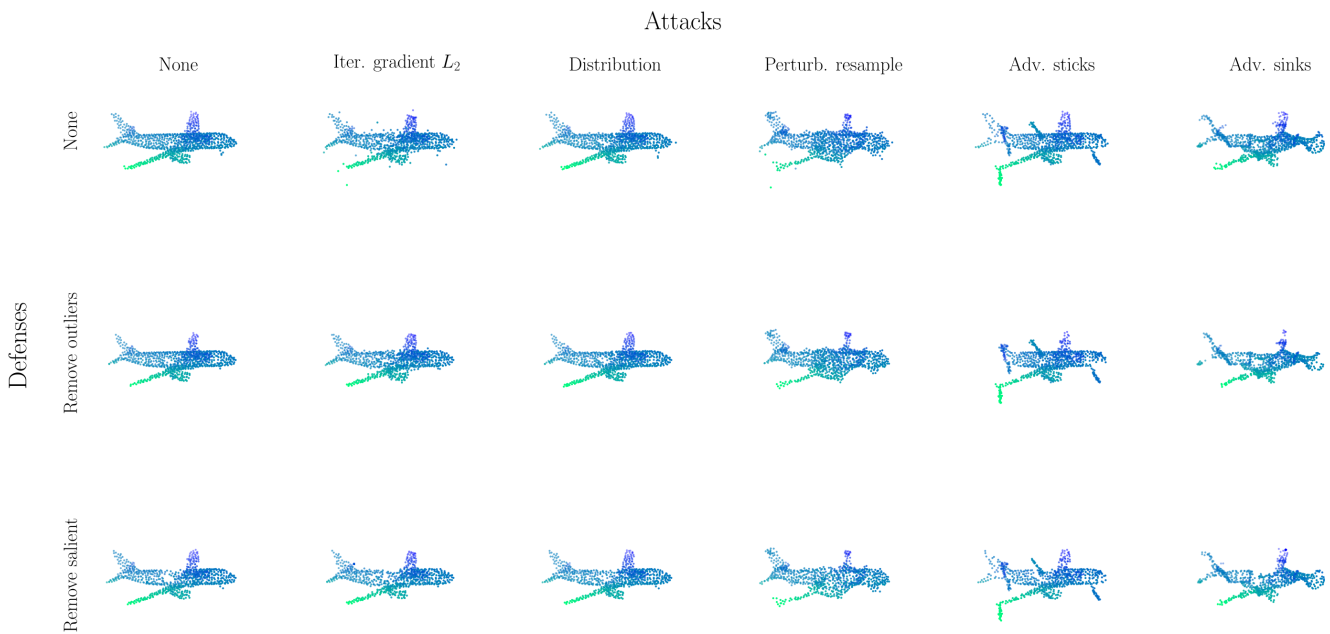


Figure 5: Visualizations of adversarial perturbations on an airplane, that are generated on the PointNet architecture, against different defensive techniques.

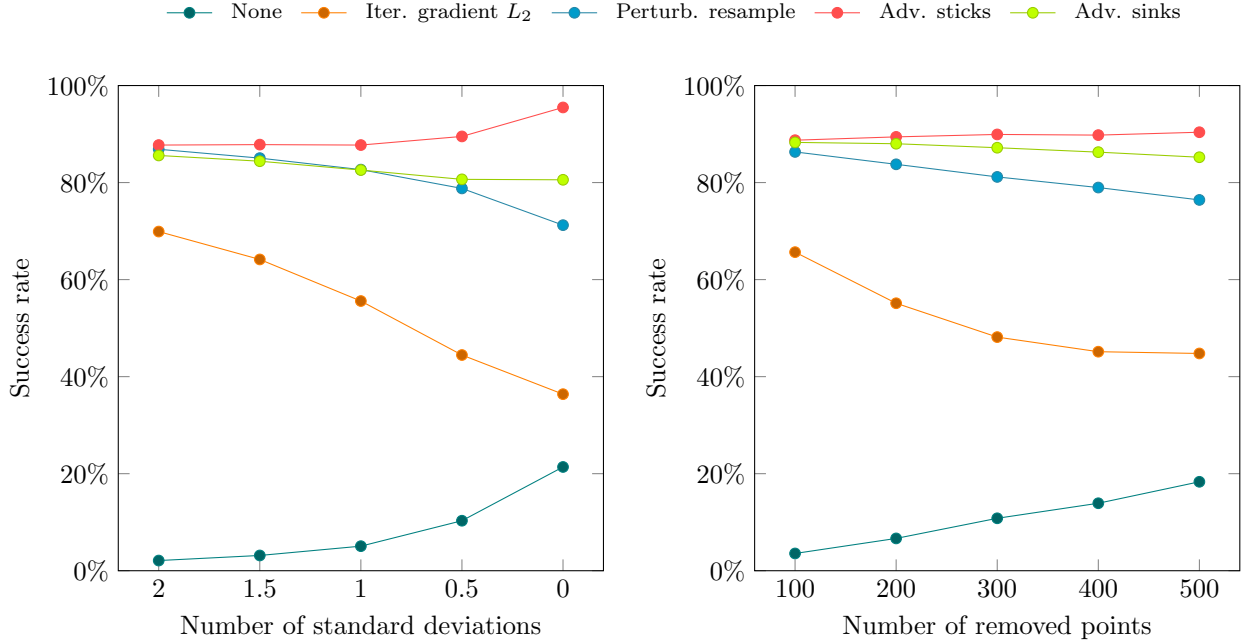


Figure 6: The success rates of adversarial attacks against the PointNet architecture as we increase the number of points removed with the outlier removal (left) and the salient point removal (right) defenses. For the outlier removal defense, more points are removed as the number of standard deviations from the average decreases.

attack increases. This is because we densely sample many points on the adversarial sticks, so they are not identified as outliers, and removing a few points based on saliency does not significantly change the sticks. Overall, most shape attacks represent a 50% to 100% increase to the success rate of iterative gradient L_2 against point removal defenses. This was expected because our shape attacks were designed to ensure that there were resampled points near points perturbed through gradient descent, so removing a few points does not restore the shape of an adversarial point cloud.

Stronger defenses. As we increase the number of points removed through the outlier removal and salient point removal defenses, we see that our three shape attacks do not experience dramatic reductions in their success rates. The shape attacks are approximately twice as successful against the defenses than the iterative gradient L_2 attack even when we remove nearly half of the points in the adversarial point clouds. Therefore, we can conclude that our shape attacks are robust against strong point removal defenses. We note that in practice, removing such a large amount of points is not recommended, as we see that removing nearly half of the points in each benign point cloud also causes PointNet to misclassify around 20% of the benign point clouds.

Perceptibility. We find that the average Hausdorff distance of the iterative gradient L_2 examples and the shape attack examples we generate on PointNet is between 0.3 and 0.4. On PointNet++, the iterative gradient L_2 , perturbation resampling and adversarial sticks attacks produce smaller perturbations between 0.1 and 0.2. For reference, each point cloud object is bounded by a unit sphere. This means that the loss wrt input gradients are smaller and the perturbations are spread out over many different points for PointNet++, compared to PointNet. Interestingly, the relatively low perceptibility of these attacks measured through the Hausdorff distance shows that within a certain amount of perturbation, we have a lot of freedom on how we want the perturbations on the shape of a point cloud to look.

The distributional attack, which attempts to bound the Hausdorff distance between approximations of the true shapes of objects and adversarial examples to $\tau = 0.05$, results in an average Hausdorff distance of 0.053 on PointNet. The slight difference is due to error when approximating the true shapes. The distributional attack also offers the best perturbation amount to adversarial attack success rate tradeoff, since it reaches 83.7% success rate on PointNet and 95.9% success rate on PointNet++ with a much lower average Hausdorff distance than other attacks. This is compared to the previously proposed gradient projection attack that results in the success rates of 26.0% on PointNet and 24.5% on PointNet++, with a Hausdorff distance of

0 [Liu et al., 2019].

Zero gradients. We find that over 30-40% of points have zero gradients (loss wrt input points) with PointNet. For a point cloud x , the number of points with zero gradients is defined as $|\{i : \|(\nabla_x J(f_\theta(x), y))[i]\|_2 < \epsilon \wedge i \in \{1 \dots N\}\}|$, for a very small ϵ value. If a point has zero gradients, then it is very likely that the point is not selected by the max pooling operation in PointNet. We see that only around 30% of the total 500 resampled points in the last iteration of the perturbation resampling attack have zero gradients, and around 50% of the total 200 resampled points in adversarial sticks have zero gradients. Since the overall (not just resampled points) average number of points that have zero gradients do not significantly change for those two resampling attacks compared to not performing any attacks, we can conclude that the resampled points are selected by the max pooling operation instead of other points. We can also conclude that our initial assumptions about the linearity of the neural networks is not too realistic in practice. Therefore, the reason the resampling attacks are effective is due to the resampled points being near points perturbed through gradient descent.

8 Conclusion

We propose four new algorithms for attacking 3D point cloud classifiers. Our experiments show that they are able to generate effective adversarial perturbations on 3D objects, even against point removal defenses that attempt to restore the adversarial examples. Our work presents new perspectives and approaches for generating adversarial attacks in 3D space. These attacks are important in better understanding the behavior of neural networks in an adversarial setting, and it gives us tools for evaluating neural networks and defensive techniques in the 3D domain.

For future work, it is important to examine defenses that do not make use of point cloud specific properties like density, as we have shown that these defenses are still vulnerable to attacks.

References

F. Bernardini, J. Mittleman, H. Rushmeier, C. Silva, and G. Taubin. The ball-pivoting algorithm for surface reconstruction. *IEEE Transactions on Visualization and Computer Graphics*, 5(4):349–359, 1999.

Y. Cao, C. Xiao, D. Yang, J. Fang, R. Yang, M. Liu, and B. Li. Adversarial Objects Against LiDAR-Based Autonomous Driving Systems. *arXiv preprint arXiv:1907.05418*, 2019.

N. Carlini and D. Wagner. Towards Evaluating the Robustness of Neural Networks. In *2017 IEEE Symposium on Security and Privacy*, pages 39–57. IEEE, 2017.

H. Deng, T. Birdal, and S. Ilic. PPF-FoldNet: Unsupervised Learning of Rotation Invariant 3D Local Descriptors. *arXiv preprint arXiv:1808.10322*, 2018.

Y. Dong, F. Liao, T. Pang, H. Su, J. Zhu, X. Hu, and J. Li. Boosting Adversarial Attacks with Momentum. *arXiv preprint*, 2018.

H. Edelsbrunner, D. Kirkpatrick, and R. Seidel. On the shape of a set of points in the plane. *IEEE Transactions on Information Theory*, 29(4):551–559, 1983.

I. Goodfellow, J. Shlens, and C. Szegedy. Explaining and Harnessing Adversarial Examples. *arXiv preprint arXiv:1412.6572*, 2014.

A. Ilyas, S. Santurkar, D. Tsipras, L. Engstrom, B. Tran, and A. Madry. Adversarial Examples Are Not Bugs, They Are Features. *arXiv preprint arXiv:1905.02175*, 2019.

D. P. Kingma and J. Ba. Adam: A method for stochastic optimization. *arXiv preprint arXiv:1412.6980*, 2014.

A. Kurakin, I. Goodfellow, and S. Bengio. Adversarial Examples in the Physical World. *arXiv preprint arXiv:1607.02533*, 2016a.

A. Kurakin, I. Goodfellow, and S. Bengio. Adversarial Machine Learning at Scale. *arXiv preprint arXiv:1611.01236*, 2016b.

D.-T. Lee and B. J. Schachter. Two algorithms for constructing a Delaunay triangulation. *International Journal of Computer & Information Sciences*, 9(3):219–242, 1980.

D. Liu, R. Yu, and H. Su. Extending Adversarial Attacks and Defenses to Deep 3D Point Cloud Classifiers. *arXiv preprint arXiv:1901.03006*, 2019.

A. Madry, A. Makelov, L. Schmidt, D. Tsipras, and A. Vladu. Towards Deep Learning Models Resistant to Adversarial Attacks. *arXiv preprint arXiv:1706.06083*, 2017.

S.-M. Moosavi-Dezfooli, A. Fawzi, and P. Frossard. DeepFool: A simple and accurate method to fool deep neural networks. In *Proceedings of the IEEE Conference on Computer Vision and Pattern Recognition*, pages 2574–2582, 2016.

S.-M. Moosavi-Dezfooli, A. Fawzi, O. Fawzi, and P. Frossard. Universal adversarial perturbations. In *Proceedings of the IEEE Conference on Computer Vision and Pattern Recognition*, pages 1765–1773, 2017.

N. Papernot, P. McDaniel, S. Jha, M. Fredrikson, Z. B. Celik, and A. Swami. The Limitations of Deep Learning in Adversarial Settings. In *2016 IEEE European Symposium on Security and Privacy (EuroS&P)*, pages 372–387. IEEE, 2016a.

N. Papernot, P. McDaniel, X. Wu, S. Jha, and A. Swami. Distillation as a Defense to Adversarial Perturbations Against Deep Neural Networks. In *2016 IEEE Symposium on Security and Privacy (SP)*, pages 582–597. IEEE, 2016b.

C. R. Qi, W. Liu, C. Wu, H. Su, and L. J. Guibas. Frustum PointNets for 3D Object Detection from RGB-D Data. *arXiv preprint arXiv:1711.08488*, 2017a.

C. R. Qi, H. Su, K. Mo, and L. J. Guibas. PointNet: Deep Learning on Point Sets for 3D Classification and Segmentation. *Proceedings of the IEEE Conference on Computer Vision and Pattern Recognition*, 1(2):4, 2017b.

C. R. Qi, L. Yi, H. Su, and L. J. Guibas. PointNet++: Deep Hierarchical Feature Learning on Point Sets in a Metric Space. In *Advances in Neural Information Processing Systems*, pages 5099–5108, 2017c.

C. Szegedy, W. Zaremba, I. Sutskever, J. Bruna, D. Erhan, I. Goodfellow, and R. Fergus. Intriguing properties of neural networks. *arXiv preprint arXiv:1312.6199*, 2013.

P.-S. Wang, Y. Liu, Y.-X. Guo, C.-Y. Sun, and X. Tong. O-CNN: Octree-based convolutional neural networks for 3D shape analysis. *ACM Transactions on Graphics*, 36(4):72, 2017.

M. Wicker and M. Kwiatkowska. Robustness of 3D Deep Learning in an Adversarial Setting. In *Proceedings of the IEEE Conference on Computer Vision and Pattern Recognition*, pages 11767–11775, 2019.

E. Wong and J. Z. Kolter. Provable Defenses against Adversarial Examples via the Convex Outer Adversarial Polytope. *arXiv preprint arXiv:1711.00851*, 2017.

Z. Wu, S. Song, A. Khosla, F. Yu, L. Zhang, X. Tang, and J. Xiao. 3D ShapeNets: A Deep Representation for Volumetric Shapes. In *Proceedings of the IEEE Conference on Computer Vision and Pattern Recognition*, pages 1912–1920, 2015.

C. Xiang, C. R. Qi, and B. Li. Generating 3D Adversarial Point Clouds. *arXiv preprint arXiv:1809.07016*, 2018.

J. Yang, Q. Zhang, R. Fang, B. Ni, J. Liu, and Q. Tian. Adversarial Attack and Defense on Point Sets. *arXiv preprint arXiv:1902.10899*, 2019.

P. N. Yianilos. Data Structures and Algorithms for Nearest Neighbor Search in General Metric Spaces. In *Soda*, volume 93, pages 311–21, 1993.

T. Zheng, C. Chen, K. Ren, et al. Learning Saliency Maps for Adversarial Point-Cloud Generation. *arXiv preprint arXiv:1812.01687*, 2018.

H. Zhou, K. Chen, W. Zhang, H. Fang, W. Zhou, and N. Yu. Deflecting 3D Adversarial Point Clouds Through Outlier-Guided Removal. *arXiv preprint arXiv:1812.11017*, 2018.